Raman spin-lattice relaxation, Debye temperature and disorder effects studied with electron spin echo of Cu^{2+} in Tutton salt crystals

2001 J. Phys.: Condens. Matter 13 7443

(http://iopscience.iop.org/0953-8984/13/33/323)

INSTITUTE OF PHYSICS PUBLISHING JOURNAL OF PHYSICS: CONDENSED MATTER

J. Phys.: Condens. Matter **13** (2001) 7443–7457 PII: S0953-8984(01)23714-X

Raman spin–lattice relaxation, Debye temperature and disorder effects studied with electron spin echo of Cu^{2+} in Tutton salt crystals

S K Hoffmann[1], **W Hilczer, J Goslar and M A Augustyniak-Jablokow**

Institute of Molecular Physics, Polish Academy of Sciences, Smoluchowskiego 17, PL-60179 Poznan, Poland

E-mail: skh@ifmpan.poznan.pl

Received 6 April 2001, in final form 20 June 2001
Published 2 August 2001
Online at stacks.iop.org/JPhysCM/13/7443

Abstract

Spin–lattice relaxation time T_1 was determined by the electron spin echo (ESE) method in the temperature range 4–60 K in a series of Tutton salt crystals $M^I_2M^{II}(SO_4)_2{\cdot}6X_2O$ (M^I = NH_4, K; M^{II} = Zn, Mg; X = H, D) weakly doped ($\leqslant 10^{18}$ ions cm^{-3}) with the $^{63}Cu^{2+}$ isotope. The ESE signal was undetectable at higher temperatures. The relaxation rate increases over the six decades in the studied temperature range with T_1 equal to 1 s at 4 K and 0.5 μs at 50 K. Various possible relaxation mechanisms are discussed with the conclusion that the relaxation is governed by two-phonon Raman processes without a noticeable contribution from the reorientations of $Cu(H_2O)_6$ octahedra between Jahn–Teller distorted configurations. Deuteration of the crystal has no effect in spin–lattice relaxation. For a few crystals, having the largest Cu^{2+} concentration among the studied crystals, a strong and linear in temperature contribution to the relaxation rate was found below 15 K. Possible explanations are discussed with the final conclusion that this effect is due to a non-uniform Cu^{2+} distribution in the host lattice producing effective relaxation via pairs and triads of the Cu^{2+} ions. From the $T_1(T)$ dependence the Debye temperature Θ_D was determined for the all crystals studied. This varies from Θ_D = 166 K for $K_2Zn(SO_4)_2{\cdot}6H_2O$ to Θ_D = 238 K for $(NH_4)_2Mg(SO_4)_2{\cdot}6H_2O$. The Θ_D values are discussed and used for calculation of the sound velocity which was found to be similar in all crystals and equal to $\nu = 4150(\pm 150)$ m s^{-1}.

1. Introduction

Electron spin relaxation in crystals is governed by many processes and mechanisms which are not easy to distinguish in experimental data. The existing theories [1, 2] allow us to evaluate roughly the value of the spin–lattice relaxation time T_1 and predict its temperature

[1] Corresponding author: Professor S K Hoffmann.

dependence for various relaxation mechanisms and processes. This does not allow us, however, to identify uniquely the processes and mechanisms. Some relaxation processes depend on the EPR resonance frequency, thus they can be identified by measurements on a few EPR frequencies. Most of the pulsed EPR spectrometers operate, however, at the X-band only. Since the relaxation measurements are performed in magnetically diluted crystals, a change in the paramagnetic centre concentration can differentiate relaxation mechanisms depending on the interaction between paramagnetic centres (like a spin diffusion).

It is expected that one of the most effective relaxation mechanisms is the vibronic dynamics of paramagnetic centres exhibiting the dynamic Jahn–Teller effect [3]. Very promising systems for studies of this mechanism are Tutton salt crystals doped with Cu^{2+} ions, especially at low temperatures where $Cu(H_2O)_6^{2+}$ complexes are close to the static Jahn–Teller limit.

Tutton salts are monoclinic crystals of general formula $M_2^I M^{II}(SO_4)_2{\cdot}6H_2O$ containing two octahedral hexyhydrate complexes $[M^{II}(H_2O)_6]^{2+}$ in the crystal unit cell (figure 1) with various divalent metal ions M^{II} and $M^I = NH_4$, K, Rb, Cs. All crystals of the family have very similar crystal unit cell dimensions and molecular structure. Special properties display the copper(II) salts and copper(II) doped salts because of the appearance of the Jahn–Teller effect (JTE). $Cu(H_2O)_2$ ions are known to be a typical example of the strong JTE both in solids and liquids [4, 5] with stabilization energy E_{JT} larger than vibrational energy $\hbar\omega$. For Cu^{2+} in Tutton salts $E_{JT} \approx 1500$ cm^{-1} and $\hbar\omega = 100$ cm^{-1} typically. The deformation of the $Cu(H_2O)_6$ octahedra in Tutton salts is larger than for hydrated Cu^{2+} complexes in water solutions since it is enhanced by crystal strains produced by hydrogen bonds between coordinated water and SO_4 groups. The strains are different along the three Cu–O directions and resulting wells in the adiabatic potential surface are strongly inequivalent as shown in figure 2. The highest energy potential well appears along shortest Cu–O(9) bond. The deepest well appears along the longest Cu–O bond, which is the Cu–O(7) bond in ammonium Tutton salts but it is the Cu–O(8) in the others. Moreover, the elongation axis is switchable between Cu–O(7) and Cu–O(8) by relatively small external pressure [6, 7] or by deuteration [8] of an ammonium salt crystals. This indicates an important role of the remote NH_4 ions in dynamic deformation of $Cu(H_2O)_6$ complexes via indirect coupling in the pathway $NH_4 \ldots SO_4 \ldots H_2O$–Cu. So the dynamics of the large cluster around the $Cu(H_2O)_6$ complex involving SO_4 groups of the second coordination sphere and NH_4 groups of the third coordination sphere competes with the JT dynamics [9].

Because of a large energy difference (between the potential wells the $Cu(H_2O)_6$ system is localized in the deepest potential well at low temperatures. This means that all $Cu(H_2O)_6$ complexes are elongated along Cu–O(7) in ammonium Tutton salts and along Cu–O(8) in non-ammonium salts. But even in this static JTE limit the zero-point motions mix $|x^2 - y^2\rangle$ and $|z^2\rangle$ wavefunctions in the ground state of elongated octahedra as we showed for Cu^{2+} in $K_2Zn(SO_4)_2{\cdot}6H_2O$ crystals [10]. Another mixing which is temperature dependent appears due to the dynamic Jahn–Teller effect as a result of jumps between potential wells (JT configuration mixing). This is observed as thermal averaging of the Cu–O bond length [11] and as an averaging of the g-factors and hyperfine splittings in EPR spectra [4, 11]. A characteristic feature of the Tutton salt crystals is that the vibronic dynamics does not influence the Cu–O bond directions, which are fixed in the whole temperature range. This vibronic dynamics is treated commonly with two simple models discussed in [4]. The models assume a two-well potential with Boltzmann population of vibronic levels. These models are valid in the intermediate temperature range (50–100 K) only. It is assumed that for higher temperatures the potential surface shape becomes temperature dependent, but the clear deviation of the model predictions at low temperatures are not understood. The low temperature vibronic dynamics including intrawell and interwell excitations can influence electron spin relaxation.

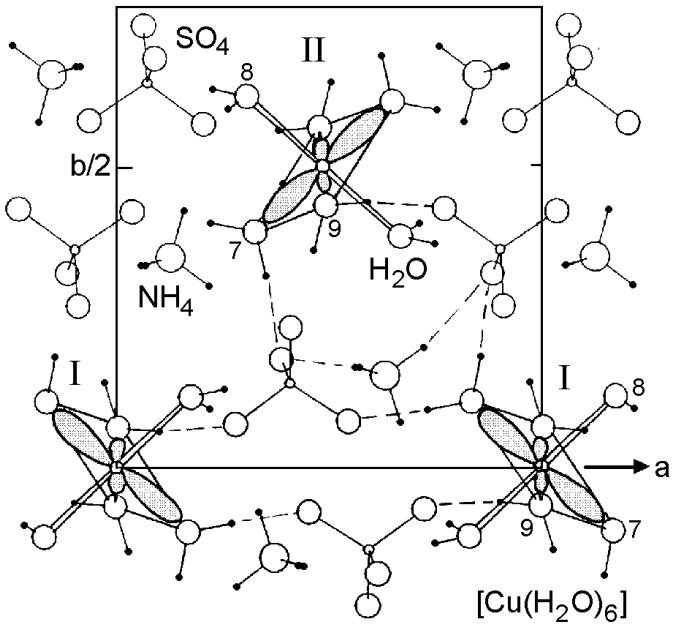

Figure 1. Crystal structure of $(NH_4)_2M^{II}(SO_4)_2{\cdot}6H_2O$ crystals in projection on the ab-plane. The doped Cu^{2+} ions replace M^{II} cations and have predominantly $|x^2 - y^2\rangle$ ground state, of which the lobes are drawn at two inequivalent positions I and II. The dotted lines mark hydrogen bonds between H_2O and SO_4 and NH_4. Room temperature unit cell dimensions for copper(II) salt ($M^{II} = Cu^{2+}$) are $P2_1/a$, $a = 9.216$ Å, $b = 12.398$ Å, $c = 6.301$ Å, $\beta = 106.12^\circ$, $Z = 2$, Cu–O(7) = 2.222 Å, Cu–O(8) = 2.070 Å, Cu–O(9) = 1.964 Å.

We have already published the pulsed EPR measurement results of Cu^{2+} ions in $(NH_4)_2Mg(SO_4)_2{\cdot}6H_2O$ [12–14], $Cs_2Zn(SO_4)_2{\cdot}6H_2O$ [15] and $K_2Zn(SO_4)_2{\cdot}6H_2O$ [10] which added new data to x-ray and CW-EPR results [8, 9]. In this paper the new results for Cu^{2+} in $(NH_4)_2Zn(SO_4)_2{\cdot}6H_2O \equiv (NH_4)_2Zn$, mixed crystals $KNH_4Zn(SO_4)_2{\cdot}6H_2O \equiv KNH_4Zn$ and deuterated crystals $K_2Zn(SO_4)_2{\cdot}6D_2O \equiv K_2ZnD$, $(ND_4)_2Mg(SO_4)_2{\cdot}6D_2O \equiv (ND_4)_2Mg$. $(ND_4)_2Zn(SO_4)_2{\cdot}6D_2O \equiv (ND_4)_2Zn$ are described and compared with the previously published data. It will be shown that the spin relaxation measurements allow us to find the Debye temperature and are sensitive to the vibronic dynamics and disorder in the studied crystals.

2. Experiments

Single crystals of $(NH_4)_2Zn$ and KNH_4Zn were grown from water solutions and K_2ZnD, $(ND_4)_2Zn$ and $(ND_4)_2Mg$ were grown from heavy water solutions. The commercially available high purity starting materials were used after additional chemical purification and several recrystallizations. Special care was taken to remove Mn^{2+} and Fe^{3+} impurities which can be easily introduced into the crystals producing cross-relaxation to intentionally doped Cu^{2+} ions and distort relaxation data especially at low temperatures.

The crystals were doped with isotope $^{63}Cu^{2+}$ by adding of about 0.1 mol% of $^{63}CuSO_4{\cdot}5H_2O$ (or D_2O) to the mother solution. The resulting concentration of Cu^{2+} ions in crystals was determined by the EPR method with respect to the ultramarine blue standard

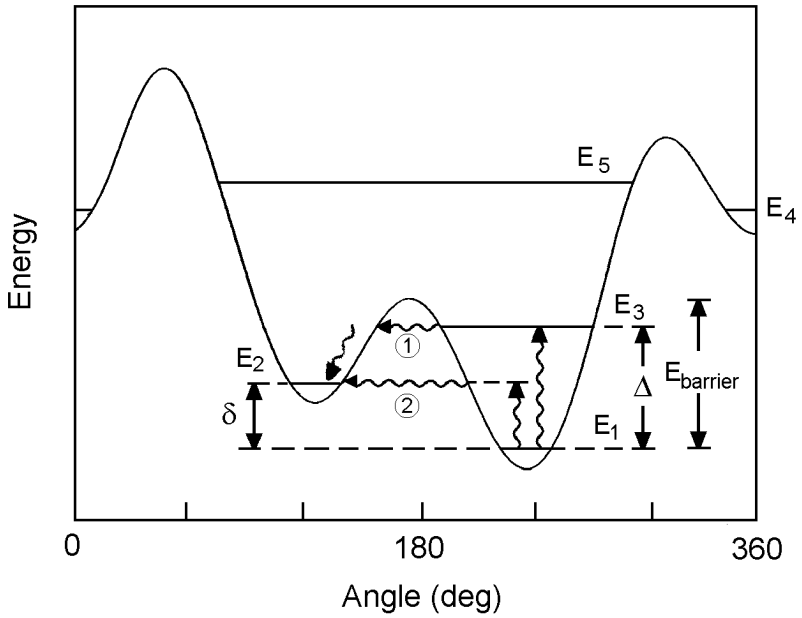

Figure 2. An angular cross-section through the adiabatic potential surface along the Jahn–Teller perimeter ρ_0 with three inequivalent wells typical for $Cu(H_2O)_6^{2+}$ vibronic complexes in Tutton salt crystals. Lattice stress produced the difference in the energy between the wells of the order of $\delta = E_2 - E_1 \approx 100\ cm^{-1}$, and $E_4 - E_1 \approx 400$–$500\ cm^{-1}$. δ is comparable with vibronic level splitting Δ. The phonon involved tunnelling processes are marked as (1) phonon-controlled process via excited vibronic state E_3 and (2) phonon-induced (assisted) process via virtual state of energy δ.

and was in the range 6×10^{17}–4×10^{18} spins g^{-1}. Final crystallization of the compounds was performed very slowly from a highly uniform solution to allow a uniform distribution of Cu^{2+} ions in the growing crystals. In fact in most crystals, but not in all, we obtain a practically uniform distribution as will be discussed later.

Mixed potassium–ammonium crystals grow easily at any K/NH_4 ratio introducing controlled disorder around divalent metal cations. In this paper we present results for $K/NH_4 = 1$.

Deuteration of crystals was performed by fivefold recrystallization from D_2O and the degree of the deuteration was determined from three-pulse ESEEM spectra, which are shown in figure 3 for $(ND_4)_2Zn(SO_4)\cdot 6D_2O$ and $K_2Zn(SO_4)_2\cdot 6D_2O$. The peaks in these ENDOR-type spectra arise from protons ^1H in the region 10–18 MHz and from deuterons D around 2 MHz. From integral intensity of the peaks we determined 79% D and 21% H in the $(ND_4)_2Zn(SO_4)\cdot 6D_2O$ crystal and a very similar D/H ratio in the $(ND_4)_2Mg(SO_4)_2\cdot 6D_2O$ crystal. In the $K_2Zn(SO_4)_2\cdot 6D_2O$ spectrum only broadened peaks from D exist, indicating practically full replacement of hydrogen atoms by deuterium atoms. These results show clearly that in the exchange-type deuteration from D_2O the ammonium groups are not fully deuterated and probably in the crystals we have (NH_xD_{4-x}) groups with various $x = 0$, 1, 2, 3, 4. It should be noted that this simple method for evaluation of the deuteron percentage has a restricted accuracy due to the Fourier transform reproducibility of the peak amplitudes, possible partial suppression of the modulations and differences in the transition probabilities for $I = 1/2$ and $I = 1$ nuclei.

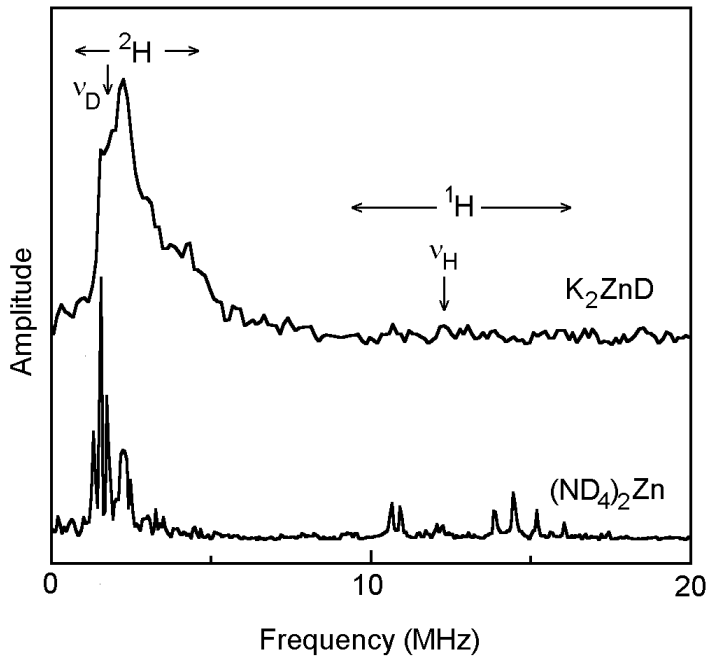

Figure 3. Three-pulse stimulated echo ESEEM spectra of deuterated compounds with marked regions of expected proton ^{1}H and deuteron ^{2}H lines, ν_H, Θ_D being proton and deuteron Larmor frequencies respectively. The spectra show that full deuteration was achieved in the $K_2Zn(SO_4)_2{\cdot}6D_2O$ compound but only 79% in $(ND_4)_2Zn(SO_4)_2{\cdot}6D_2O$, where ammonium groups were only partially deuterated.

Pulsed EPR experiments were performed on a Bruker ESP 380E FT/CW spectrometer with a dielectric TE^{001} resonator, equipped with a helium flow OXFORD CF935 cryostat. The temperature dependence of the relaxation rate was measured on the low-field hyperfine EPR line ($m_I = -3/2$) along the local z-axis of the $Cu(H_2O)_6^{2+}$ octahedra (z-axis of the **g** and **A** tensors) (see the inset in figure 4). During pulsed EPR experiments the whole hyperfine line was excited and the exciting pulse duration was 16 or 24 ns (spectral width 22.3 and 14.9 G respectively) for protonated compounds and 240 ns (1.5 G spectral width) for $K_2Zn(SO_4)_2{\cdot}6D_2O$. The FID signal was not observed and we used an electron spin echo (ESE) signal of Hahn type excited by two equal pulses with interpulse interval 120 ns. Microwave power was adjusted to maximize the ESE signal, i.e. to obtain $2/3\pi$ pulses.

The electron spin–lattice relaxation time was determined using the saturation recovery method with monitoring of the magnetization recovery by the ESE signal. The full saturation was achieved by a 24 ns pulse in the $(NH_4)_2Zn$ crystal, 40 ns in (ND_4) crystals and a 48 ns pulse in the K_2ZnD crystal. The recovery signal was a single exponential in the whole temperature range for all the studied crystals. We have checked whether the T_1-value depends on the microwave power and pulse width. A small dependence on the power was observed below 18 K, indicating that ESE decay is determined to some degree by instantaneous diffusion. The three-pulse stimulated ESE signal was recorded with time interval $\tau = 136$ ns for a further Fourier transform giving ENDOR-type spectra shown in figure 3.

The ESE signal was detectable below 60 K. For higher temperatures the dephasing rate was so fast that the ESE signal was hidden in the dead time of the pulsed spectrometer.

3. Results and discussion

3.1. Temperature dependence of the relaxation rate and relaxation mechanisms

The electron relaxation of Cu^{2+} in our compounds is relatively slow at helium temperatures with T_1 of the order of seconds, and accelerates rapidly on heating over six decades in the temperature range 4–60 K. This is typical behaviour when the relaxation is governed by phonon processes below the Debye temperature. Various phonon processes and phonon-stimulated mechanisms can contribute to spin relaxation. Ordinary phonon processes operating mostly in ionic crystals via an orbit–phonon mechanism lead to a relaxation rate which depends on the temperature as

$$\frac{1}{T_1} = A_{dir}T + A_{Raman}T^9 I_8 + A_{Orbach}\Delta^3 \exp\left(-\frac{\Delta_{orbital}}{kT}\right). \tag{1}$$

The first term describes the direct one-phonon process. The T^9-term describes the two-phonon Raman process with transport integral $I_8(\Theta_D/T)$ over the Debye-type phonon spectrum. This term is written for Kramers-type transitions as for Cu^{2+} ions and the I_8-integral has the form

$$I_8 = \int_0^{\Theta_D/T} \frac{x^8 \exp(x)}{[\exp(x)-1]^2}\,\mathrm{d}x \tag{2}$$

where Θ_D is the Debye temperature. We have found previously an analytical approximation of I_8 useful in computer fitting procedures [16]. The last term describes the resonance-type relaxation via an excited orbital level (Orbach–Aminov process) of energy $\Delta_{orbital}$, which is expected when $\Delta_{orb} < k\Theta_D$, which, however, is not the case for Cu^{2+} ions in octahedral crystal fields.

The spin–lattice relaxation can be also driven by mechanisms specific for Jahn–Teller systems. A few types of contribution to $1/T_1$ can be expected. The first is related to the vibronic nature of the energy levels having mixed vibrational–electronic wavefunctions. Excitations to these levels (see figure 2) of energy E_i will produce an effect described by the following equation:

$$\frac{1}{T_1} = \sum_i A_{vibronic} \exp\left(-\frac{\Delta_i}{kT}\right). \tag{3}$$

This equation has a form similar to the Orbach–Aminov term in equation (1) but because of much smaller Δ_i as compared to $\Delta_{orbital}$ the population of the Δ_i must be taken into consideration, which leads to the equation $1/T_1 \propto \mathrm{cosech}(\Delta_i/kT)$ as in the Murphy mechanism [17] with equation (3) being the low temperature approximation only, when $\Delta_i > kT$.

Another contribution is expected from thermally activated reorientations between potential wells. At low temperatures the reorientation rate $1/\tau_r$ can be determined by tunnelling from the ground state which for $kT > \delta$ (δ is the energy difference between the wells—figure 2) via a phonon assisted Δ_i induced) tunnelling mechanism (see mechanism (2) in figure 2) gives [18]

$$\frac{1}{\tau_r} = a_1|3\Gamma|^2 T + b_1|3\Gamma|^2 T^3 I_2(\Theta_D/T) \tag{4}$$

where 3Γ is the tunnelling splitting. Under dynamic Jahn–Teller conditions when a dynamic averaging of EPR spectra appears [3] the overlap between vibronic states of neighbouring wells leads to the reorientational rate

$$\frac{1}{\tau_r} = a_2\delta^3 T + b_2 T^5 I_4(\Theta_D/T). \tag{5}$$

Equations (4) and (5) are written for simplicity in the high temperature approximation i.e. when the thermal energy is larger than the inequivalence δ between potential wells and much larger than the Zeeman splitting ($g\mu_B B < \delta < kT$). For low temperatures τ_r is calculated as a Boltzmann average value for all occupied states in considered wells. At temperatures comparable or higher than Δ/T the phonon-controlled tunnelling via vibronic state of energy Δ can be effective (see mechanism (1) in figure 2) with [19]:

$$\frac{1}{\tau_r} = \nu_{tunnel} \exp\left(-\frac{\Delta}{kT}\right) \tag{6}$$

where $\nu_{tunnel} = (3\Gamma/\hbar)$ is the tunnelling frequency of the order of 10^7 s^{-1} [20]. This equation is a simplified form for a phonon-controlled tunnelling process at low temperatures when $kT \ll \Delta$ and is simply a product of thermal excitations probability and tunnelling probability. In the case of inequivalent potential well with energy difference δ and for finite spectral width $\Delta\varepsilon$ of the excited vibronic level the general formula for the phonon-controlled reorientation rate is [21]

$$\frac{1}{\tau_r} = \frac{4\Gamma^2\Delta\varepsilon}{\Delta\varepsilon^2 + 4\delta^2}\left(1 + \frac{\Delta}{kT}\right)^{-1}. \tag{7}$$

For even higher temperatures the overbarrier jumps can contribute with

$$\frac{1}{\tau_{jumps}} = \nu_{vibr} \exp\left(-\frac{E_{barrier}}{kT}\right) \tag{8}$$

where ν_{vibr} is the vibrational frequency of the order of 10^{13} s^{-1} and $E_{barrier}$ is the barrier height of the order of 400 cm^{-1} in Tutton salts. Equations (3), (6) and (8) have very similar form typical for a thermally activated process and differ in preexponential factor only. This factor is of the order of the vibrational frequency (10^{13} s^{-1}) in (3) and (8) and of the order of the tunnelling frequency (10^7 s^{-1}) in (6). This allows us to distinguish between them assuming that the overbarrier jumps can contribute at higher temperatures only when $kT \approx E_{barrier}$.

The reorientations between potential energy minima described by equations (8) and (9) can produce direct [21] or indirect [3] spin flips (spin relaxation). The former is due to a direct spin–orbit coupling between vibronic states of neighbouring wells with $T_1 = \tau_r$, whereas the latter results from a modulation of anisotropic g-tensor and hyperfine splitting by the reorientations with $1/T_1 < 1/\tau$. For $kT < \delta$ the relationship between T_1 and τ_r is [3]

$$\frac{1}{T_1} = \frac{2}{3}\left[\frac{\Delta g\mu_B B + \Delta A m_1}{h\nu}\right]^2 (k^2l^2 + l^2m^2 + m^2k^2)\frac{1}{\tau_r} \tag{9}$$

where $\Delta g = g_\parallel - g_\perp$, $\Delta A = A_\parallel - A_\perp$, m_I is the magnetic quantum number of hyperfine levels and k, l, m are direction cosines of the magnetic field $\boldsymbol{B}$ in the g-tensor principal axis system.

We have considered all the above possible contributions in analysis of the experimental data presented in figure 4 and figure 5. In some compounds the linear $1/T_1(T)$ dependence was observed at low temperatures and this will be discussed in the next section. The observed temperature dependence of the $1/T_1$ rate was faster than predicted by the T^3 and T^5 type dependence, indicating that contributions from the mechanisms described by equations (4) and (5) are negligible. Orbach type relaxation (equation (1)) is not expected for Cu^{2+} ions and overbarrier jumps do not exist below 60 K in Tutton salts. Thus, we have analysed the temperature dependences with Raman processes and exponential type contributions (equations (3) and (6)) described by

$$\frac{1}{T_1} = a + bT + cT^9 I_8(\Theta_D/T) + a_1 \exp\left(-\frac{\Delta_1}{kT}\right) + a_2 \exp\left(-\frac{\Delta_2}{kT}\right). \tag{10}$$

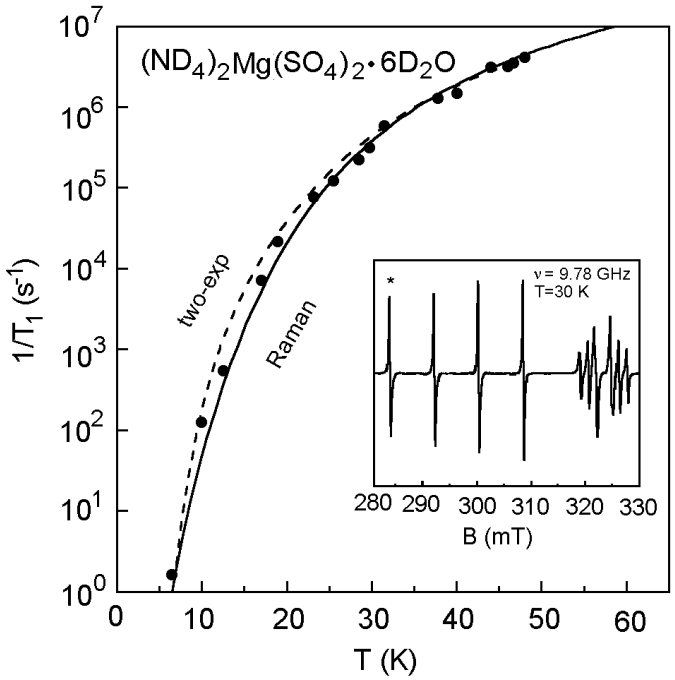

Figure 4. Temperature dependence of the spin–lattice relaxation rate $1/T_1$ of Cu^{2+} in an $(ND_4)_2Mg(SO_4)_2 \cdot 6D_2O$ crystal. Experimental points were fitted with the equation describing the two-phonon Raman process and with a sum of two exponential functions describing the possible excitations to the higher energy vibronic levels. The former possibility is favoured as discussed in the text. The inset shows the EPR spectrum with the hyperfine line for which pulsed EPR experiments were performed marked with an asterisk.

The temperature independent term is equal to zero ($a = 0$) in all compounds, indicating no contribution from spectral or spin diffusion and no cross-relaxation to impurities.

We have found that the experimental $1/T_1(T)$ dependencies can be fitted nearly equally well using only a Raman term or using only two terms with exponential functions in equation (10). A comparison of those two fits for the $(ND_4)_2Mg(SO_4)_2 \cdot 6D_2O$ crystal is shown in figure 4. Both fits give reasonable parameters: for the Raman term, $b = 0$, $c = 1.4 \times 10^{-12}$ K^{-9} s^{-1}, $\Theta_D = 238$ K; for two exponents, $b = 0$, $a_1 = 4 \times 10^6$ s^{-1}, $\Delta_1 = 106$ K $= 70$ cm^{-1}, $a_2 = 2 \times 10^8$ s^{-1}, $\Delta_2 = 195$ K $= 135$ cm^{-1}. There exist two arguments, however, which strongly favour the first alternative. The first argument is given by the relaxation data of the non-Jahn–Teller ion Mn^{2+} in $(NH_4)_2Mg(SO_4)_2 \cdot 6H_2O$ [14]. The relaxation of Mn^{2+} cannot be produced by the vibronic mechanism, since no Jahn–Teller effect operates in $Mn(H_2O)_6$ complexes, but is well described by a Raman process with Debye temperature $\Theta_D = 238$ K, which is exactly the same as for the deuterated analogue in this paper. The second argument results from the fact that two exponential functions must be used in computer fits, whereas the single function does not fit the experimental results. The first exponential function describes relaxation via the first excited vibronic level $E_3 = 70$ cm^{-1} whereas the second exponential function describes relaxation via the second energy level $E_5 = 135$ cm^{-1} (figure 2). These energies seem to be small as compared with data published for Cu^{2+} in Tutton salt crystals [4]. Moreover, the hypothetical state E_5 should be located close to the barrier top of the deepest well or delocalized between two wells as in figure 2. In both

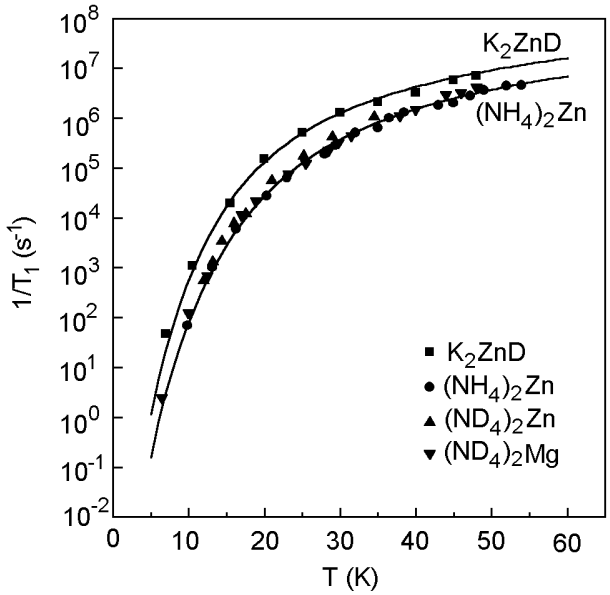

Figure 5. Temperature dependence of $1/T_1$ for the four Tutton salts with solid lines describing the Raman relaxation process with parameters given in table 1.

Table 1. Spin–lattice relaxation parameters of Cu^{2+} in Tutton salt crystals $M_2^I M^{II}(SO_4)_2{\cdot}6H_2O$: $1/T_1 = bT + cT^9 I_8(\Theta_D/T)$.

Compound $M_2^I M^{II}$	Concentration (spins cm^{-3})	Temperature range [K]	b (K^{-1} s^{-1})	c (K^{-9} s^{-1})	Θ_D [K]	Ref.
K_2Zn	1.4×10^{18}	8–50	0	14.4×10^{-12}	166	[10]
K_2ZnD	1.2×10^{18}	7–28	0	14.5×10^{-12}	166	This work
$(NH_4)_2Zn$	1.6×10^{18}	16–54	0	2×10^{-12}	201	This work
$(ND_4)_2Zn$	1.6×10^{18}	18–35	0	2.9×10^{-12}	201	This work
$K(NH_4)Zn$	2.0×10^{18}	6–55	540	0.85×10^{-12}	211	This work
$(NH_4)_2Mg$	4.0×10^{18}	19–53	1700	0.8×10^{-12}	238	[12, 14]
$(ND_4)_2Mg$	2.0×10^{18}	6–48	0	1.2×10^{-12}	238	This work
Cs_2Zn	8.0×10^{18}	10–50	210	1.4×10^{-12}	220	[15]

Errors: b and c, 8% Θ_D, ± 3 K.

cases the strong dynamical averaging of EPR spectra of the two wells should be observed with a full averaging in the latter case. We observe an onset of such behaviour only in our crystals at the temperature range where T_1 was determined. Thus, we conclude that the spin–lattice relaxation is dominated by two-phonon Raman processes for Cu^{2+} in all Tutton salt type crystals and the relaxation parameters are summarized in table 1, where data for other Tutton salts studied by us previously, are added. The data of the table and figures 4, 5 and 6 show that the temperature behaviour of the relaxation rate is very similar for Cu^{2+} in the all studied compounds. A slightly faster (two-fold) relaxation exists in K_2Zn and K_2ZnD crystals due to the smaller Debye temperature. Deuterization does not affect the Raman relaxation mechanism at all. The coefficient c in the Raman term of equation (10) describing the electron–phonon coupling strength is of the order of 10^{-12} K^{-9} s^{-1} typical for molecular crystals.

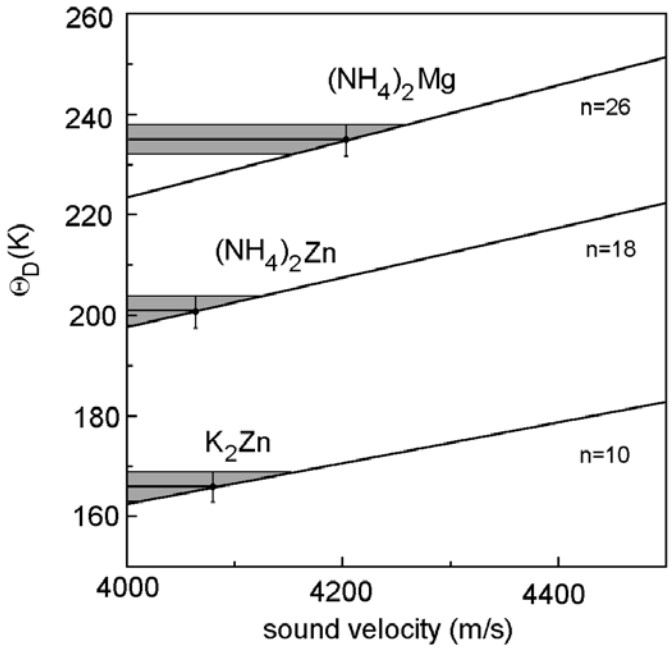

Figure 6. The Debye temperature Θ_D against the sound velocity calculated for Tutton salt crystals with n being the number of vibrating units in the crystal unit cell. Experimentally determined Θ_D values (table 1), shown by the shaded areas, fit calculations for different n.

3.2. The Debye temperature Θ_D

The Debye temperatures Θ_D shown in table 1 were determined from a computer fitting procedure using c and Θ_D of equation (1) as free parameters. Equation (1) assumes the Debye-type phonon spectrum with cut-off frequency $\omega_{max} = \omega_D = k\Theta_D/\hbar$. The Debye-type density $\rho(\omega)$ of phonon states is included in the transport integral I_8 (equation (2)). To write down the $\rho(\omega)$ contribution in an open form one can rewrite the I_8 integral over the phonon frequencies as

$$\int_0^{\omega_D} \rho^2(\omega) f \cdot (f+1)\omega^2 \cdot \omega^2 \, \mathrm{d}\omega. \tag{11}$$

The $\rho^2(\omega)$ results from the Raman process involving two phonons having the difference in frequency equal to electron Larmor frequency. This difference is negligible as compared to the phonon frequencies. The $f(f+1)\omega^2$ results from boson statistics of phonons with occupation number $f = [\exp(\hbar\omega/kT) - 1]^{-1}$, and the last ω^2 results from orbit–lattice coupling for Kramers transitions i.e. for Cu^{2+} ions.

In the Debye model $\rho(\omega) \propto \omega^2$ and the integrand in equation (11) contains ω^8-dependence. Some modifications of $\rho(\omega)$ have been proposed in special cases for a better description of experimental data [22–24]. A general modification has not been proposed although it is well known that the Debye model is only a crude approximation of the real phonon spectra even for metals and simple ionic crystals. Despite this, the model is still widely used with Θ_D being an effective parameter characterizing phonon spectrum even in amorphous and biological materials. The best way to determine Θ_D are measurements of the Debye–Waller factor in inelastic neutron scattering experiments, but mostly the Θ_D is determined from specific heat measurements (calorimetric Θ_D) and from elastic constant of a crystal measured in ultrasonic

or Brillouin scattering experiments (elastic Θ_D). As a rule, these values are not identical and differ from spectroscopic Θ_D determined from EPR relaxation data [16].

Phonon spectra and dispersion phonon curves $\omega_{ph}(k)$ are not available for Tutton salts and only crude evaluations of Θ_D were published as 100 K for the lower Θ_D limit [25] and $\Theta_D \approx 10^3$ K from the high-temperature limit for Raman processes with $\Theta_D = T$ where the T^2-dependence starts [26]. Our results are of much higher accuracy since the whole temperature dependence of T_1 relaxation time was used, which involved the whole phonon spectrum up to 8×60 K $= 480$ K (in the temperature range up to 60 K).

The Debye temperature can be simply evaluated in the Debye elastic continuum approximation as [16]

$$\theta_D = \frac{h}{k} v_L v_T \left(\frac{9}{4\pi} \frac{n}{V_n} \frac{1}{2v_L^3 + v_T^3} \right)^{1/3} \tag{12}$$

where v_L and v_T are longitudinal and transversal acoustic wave velocities propagating in a crystal with n vibrating units (atoms, molecules) in the crystal unit cell of volume V_u. The sound velocities are not known for Tutton salt crystals. Typical values for molecular crystals are $v_L \approx 4000$–5000 m s^{-1} and $v_T \approx v_L/2$. For the $(NH_4)_2Mg(SO_4)_2{\cdot}6H_2O$ crystal $V_u = 0.695 \times 10^{-27}$ m^3 whereas for $K_2Zn(SO_4)_2{\cdot}6H_2O$ $V_u = 0.654 \times 10^{-27}$ m^3 with a respective number of atoms in the unit cell of $n = 78$ and $n = 62$ (for $Z = 2$). For such n-values and $v_L = 2v_T = 3000$–5000 m s^{-1} the calculated Debye temperature is $\Theta_D > 300$ K, which is much higher than the measured values. This means that not the individual atoms but molecular groups as a whole are involved in lattice vibrations, similarly as we observed in glycine compounds [16]. So, we can assume that the vibrating units are $[Cu(H_2O)_6]$, SO_4 and K in $K_2Zn(SO_4)_2{\cdot}6H_2O$ crystal with $n = 10$. In the ammonium compound the hydrogen atoms of NH_4-groups are involved in strong and partially bifurcated hydrogen bonds with SO_4 groups and NH_4 groups cannot be treated as vibrating units. Taking all atoms of NH_4 separately we have $n = 26$ whereas, for independent vibrations of the strongest hydrogen bonds we have $H + H + NH_2$ and $n = 18$. Results of calculations and our experimental data are compared in figure 6. It is clearly seen that the low Θ_D for K_2Zn crystal results from the lower number of atoms in the crystal unit cell (lower crystal density) and the results fit with $n = 10$ for vibrating K atoms, SO_4 and $[Zn(H_2O)_6]$ groups. The Θ_D for ammonium compounds is higher and the data fit well with $n = 26$ for Mg compounds and $n = 18$ for the Zn compound. The origin of this difference is not clear. The general conclusion is that sound velocity is $4150(\pm 150)$ m s^{-1} in Tutton salt crystals.

It should be stressed that our Θ_D values were determined from dynamic properties of admixtures of Cu^{2+} ions substituting for host Zn^{2+} ions. Thus, we can expect that Θ_D does not necessarily reflect the host lattice phonon spectrum. This effect may be partially responsible for the difference in Θ_D values for various compounds in table 1, especially since $Cu(H_2O)_6$ complexes differ also in Jahn–Teller dynamics.

3.3. Crystal disorder effects in the spin–lattice relaxation

An inspection of table 1 shows that only three of the compounds have non-zero bT-term in the temperature dependence of the relaxation rate. Such a linear dependence is usually treated as due to the direct single-phonon relaxation process. Such a process, however, is expected to dominate at low temperatures where $kT \leqslant g\mu_B B$ and was found to be dominating and frequency dependent below 2.11 K for Cu^{2+} in the $(NH_4)_2Zn$ crystal [27]. In our compound, however, the linear dependence dominates up to 15 K. Moreover, the relaxation rate is rather high with $b > 200$ K^{-1} s^{-1} being larger than expected for the mechanism of the ligand

field modulation by phonons. This suggest that the linear increase of the relaxation rate with temperature is produced by different relaxation mechanisms. Such a dependence can be expected in an intermediate temperature range for the following relaxation mechanisms. (a) In the spin–orbit phonon induced (assisted) process as described by equation (6). (b) Relaxation through exchange coupled clusters of Cu^{2+} ions when there exists an inhomogeneous distribution of doped Cu^{2+} ions or when the ion concentration is too high. (In Tutton salts the Cu–Cu pair spectrum becomes EPR detectable for Cu^{2+} concentration higher than 4 mol%.) The mechanism of relaxation is the modulation of intercluster exchange interaction by phonons with random distribution of singlet–triplet splitting J. The single ions relax via spin diffusion or cross-relaxation to fast relaxing pairs, triads or larger clusters [25, 28, 29]. This mechanism leads to the quadratic dependence of $1/T_1$ at very low temperatures when $kT < J$ and to linear dependence at higher temperatures. (c) Local vibration mode effects involving tunnelling motion of molecular groups or their torsional oscillations (Murphy mechanism) [17, 30, 31]. In such a case $1/T_1 \propto \mathrm{cosech}(\Delta/kT)$ where Δ is the tunnelling splitting. This dependence is approximately linear for $kT > \Delta$. (d) Interaction between tunnelling two-level systems (TLSs) and unpaired electrons effective in amorphous materials, which gives $1/T_1 \propto T^2$ at low temperatures and $1/T_1 \propto T$ at higher temperatures (above 10 K) [17, 22, 32, 33].

The mechanisms (b), (c) and (d) are dominant in electron spin–lattice relaxation in amorphous, disordered and glassy solids where phonon mechanisms are not effective. The mechanisms (a), (c) and (d) are effective enough to produce similar effects in the spin–lattice relaxation of Cu^{2+} in all Tutton salt crystals except a few. Thus, mechanism (b) seems to be responsible for linear relaxation rate dependence at low temperatures in $(NH_4)_2Mg$, Cs_2Zn and $K(NH_4)Zn$ crystals. Disorder in the Cu^{2+} ion distribution can be introduced into the growing crystals as a result of uncontrolled fluctuations in inhomogeneity of the mother solution or an instability in growing conditions. Moreover, the concentration of Cu^{2+} in these crystals is slightly higher than in others despite the identical Cu^{2+} concentration in the mother solution.

Another type of disorder in our crystals can be artificially introduced and controlled by a mixing of various M^I ions in the same crystal lattice. The mixed crystals of the type $K_x(NH_4)_{2-x}(SO_4)_2{\cdot}6H_2O$ can be grown for the whole range of $x = 0$–2. The maximal disorder is expected at $x = 1$ when potassium and ammonium ions are randomly distributed over the M^I sites. This means that in the third coordination sphere of Cu^{2+} different numbers of K and NH_4 are located at different crystal sites. These ions influenced differently the geometry of vibronic $Cu(H_2O)_6$-complexes via the hydrogen bond system. As a result, the differently deformed complexes exist in the crystal with random distribution of the EPR g-factors and δ splittings. This results in an asymmetrical and temperature dependent EPR line shape as we described in detail recently [34]. For a predominant number of NH_4 the elongation of $Cu(H_2O)_6$ octahedra along the Cu–O(7) axis is preferred, whereas for a predominant number of K ions the Cu–O(8) elongation appears. As a result, in the KNH_4Zn crystal instead of two EPR spectra from I and II complexes (see figure 1) four spectra coexist from I and II sites of K and NH_4 types. This is clearly seen in the angular variation of the resonance line positions presented in figure 7. Because of the good separation of the lines from K and NH_4-type complexes in their elongation directions we were able to make relaxation measurements separately on the $m_I = -3/2$ lines (asterisk in the inset of figure 4). The results are shown in figure 8, where they are compared with results for K_2Zn and $(NH_4)_2Zn$ compounds. Two effects can be seen. The relaxation rate is practically the same for both types of complex in the whole temperature range. This indicates that the two-phonon mechanism of the relaxation is not strongly disturbed by internal local dynamics of $Cu(H_2O)_6$ complexes. Moreover, the linear temperature dependence of $1/T_1$ is observed at low temperatures. This dependence can result from two effects. The first one is a nonuniform Cu^{2+} distribution resulting in mechanism (b)

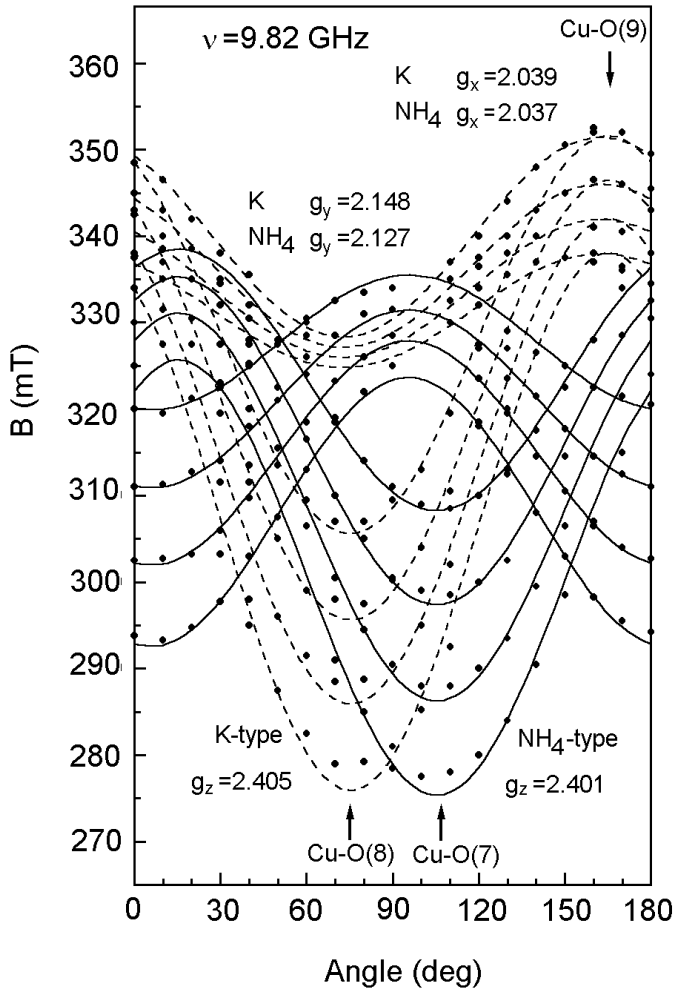

Figure 7. Angular variations of the EPR spectrum of the mixed $KNH_4Zn(SO_4)_2{\cdot}6H_2O$:^{63} Cu^{2+} compound in the crystal plane perpendicular to the $[3\bar{2}3]$ direction at 10 K. In this plane the principal axis directions of the g-tensor for I and II Cu^{2+} complexes are located. Two sets of two magnetically inequivalent complexes exist: solid lines for NH_4-type complexes and dashed lines for K-type complexes having the main elongation axis along Cu–O(7) and Cu–O(8), respectively (see figure 1).

and the second one can be due to the mechanism (d). In the latter one the $Cu(H_2O)_6$ complexes can tunnel between states with different deformations of the same Jahn–Teller configuration leading to relaxation similar to that of TLS in amorphous materials. The contributions from both mechanisms cannot be separated in our experimental data.

4. Conclusions

Electron spin–lattice relaxation of Cu^{2+} in Tutton salts is overdominated by ordinary two-phonon Raman processes although a significant effect from interwell vibronic dynamics could be expected according to suggestions of some rather old papers [25, 26]. This dynamics

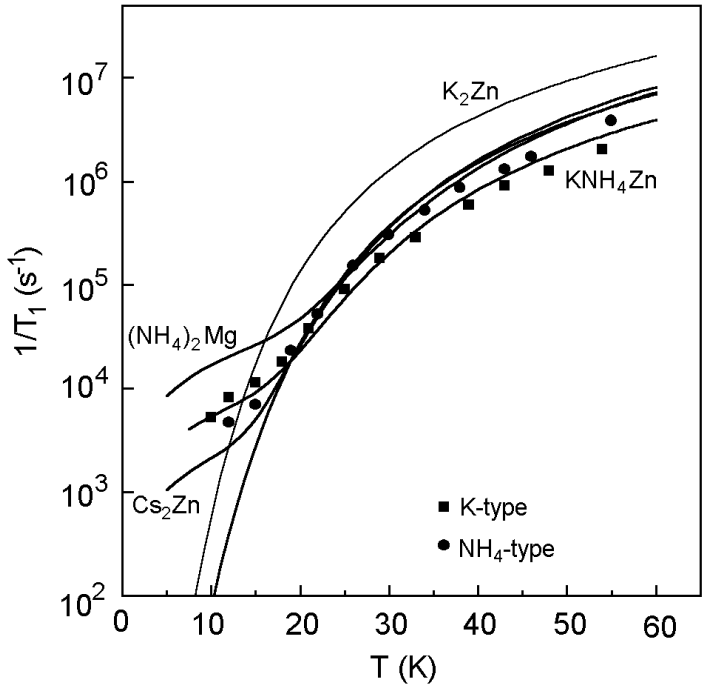

Figure 8. Temperature dependence of the relaxation rate $1/T_1$ for the mixed KNH_4Zn compound (points) compared with the data for the other compounds summarized in table 1. Disorder effects produce strong acceleration of the relaxation at low temperatures for $(NH_4)_2Mg$, CsZn and the mixed crystals.

is detectable by cw-EPR as g-factor and hyperfine splitting averaging and is also the main source of temperature dependent dephasing of the electron spin echo signal as we suggested previously [10, 15]. For some compounds having only slightly higher Cu^{2+} concentration than other crystals of the studied series the relaxation at low temperatures was found to be strongly accelerated with linear dependence on temperature below 15 K. This is due to a nonuniform distribution of Cu^{2+} in the host crystal lattice despite a rather low Cu^{2+} concentration of the order of 10^{18} ions cm^{-3}. Proof of this effect was possible only because we collected results for a series of isostructural compounds. We observed a similar effect in the mixed crystals where disorder was intentionally introduced in the monovalent cation sublattice.

We expected an isotope effect after the substitution of hydrogen atoms by heavier deuterium atoms. However, within experimental accuracy, we have found no effect on the spin relaxation. This indicates that phonon spectra are not very sensitive to deuteration in molecular ionic crystals of Tutton salt type.

We have shown that electron spin–lattice relaxation data delivering the Debye temperature value allow us to evaluate, with good accuracy, the sound velocity in single crystals.

Acknowledgments

This work was supported by the Polish Scientific Research Committee under grant KBN-2-P03B-122-14.

References

[1] Orbach R 1972 *Electron Paramagnetic Resonance* ed S Geschwind (New York: Plenum) ch 2
[2] Bowman M K 1979 *Time Domain Electron Spin Resonance* ed L Kevan and R N Schwartz (New York: Wiley) ch 3
[3] Ham F S 1972 *Electron Paramagnetic Resonance* ed S Geschwind (New York: Plenum) ch 1
[4] Riley M J, Hitchman M A and Mohammed A W 1987 *J. Chem. Phys.* **87** 3766
[5] Beagley B, Eriksson A, Lindgreen J, Persson I, Pettersson L G M, Sandstrom M, Wahlgren U and White E W 1989 *J. Phys.: Condens. Matter* **1** 2395
[6] Simmons C J, Hitchman M A, Stratemeier H and Schultz A J 1993 *J. Am. Chem. Soc.* **115** 11 304
[7] Augustyniak M A and Krupski M 1999 *Chem. Phys. Lett.* **311** 126
[8] Henning R W, Schultz A J, Hitchman M A, Kelly G and Astley T 2000 *Inorg. Chem.* **39** 765
[9] Augustyniak M A and Usachev A E 1999 *J. Phys.: Condens. Matter* **11** 4391
[10] Hoffmann S K, Goslar J, Hilczer W and Augustyniak-Jablokow M A 2001 *J. Phys.: Condens. Matter* **13** 707
[11] Bebendorf J, Burgi H B, Gamp E, Hitchman M A, Murphy A, Reinen D, Riley M J and Stratemeier H 1996 *Inorg. Chem.* **35** 7419
[12] Hoffmann S K, Goslar J, Hilczer W, Augustyniak M A and Marciniak M 1998 *J. Phys. C: Solid State Phys.* A **102** 1697
[13] Goslar J, Hilczer W and Hoffmann S K 1998 *Inorg. Chem.* **37** 5936
[14] Hoffmann S K, Augustyniak M A, Goslar J and Hilczer W 1998 *Mol. Phys.* **95** 1265
[15] Hoffmann S K, Goslar J, Hilczer W, Kaszynski R and Augustyniak-Jablokow M A 2001 *Solid State Commun.* **117** 333
[16] Hoffmann S K, Hilczer W and Goslar J 1996 *J. Magn. Res.* A **122** 37
[17] Murphy J 1966 *Phys. Rev.* **145** 241
[18] Pirc R, Zeks B and Gosar P 1966 *J. Phys. Chem. Solids* **27** 1219
[19] Sussmann J A 1967 *J. Phys. Chem. Solids* **28** 1643
[20] Sturge M D 1968 *Solid State Physics* vol 20, ed F Seitz, D Turnbull and H Elvenreich (New York: Academic) pp 91–211
[21] Vikhnin V S 1978 *Fiz. Tverd. Tela* **20** 1340
[22] Stevens S B and Stapleton H J 1990 *Phys. Rev.* B **42** 9794
[23] Korradi G, Polyar K, Vikhnin V S, Dovchenko L G and Zaritskii I M 1984 *Fiz. Tverd. Tela* **26** 252
[24] Raghunathan P 1991 *Chem. Phys. Lett.* **182** 331
[25] Gill J C 1975 *J. Phys.* C **8** 4203
[26] Jain V K, Vugman N V and Yadan V S 1988 *Phys. Rev.* B **37** 9716
[27] Pratt T E 1969 *Phys. Rev.* A **177** 664
[28] Misra S K 1998 *Spectrochim. Acta* A **54** 2257
[29] Al'tshuler S A and Kozyrev B M 1972 *Electron Paramagnetic Resonance of Transition Metal Compounds* (Moscow: Nauka) pp 216–166
[30] Dalton L R, kWiram A L and Cowen J A 1972 *Chem. Phys. Lett.* **17** 495
[31] Michalik J and keVan L 1978 *J. Chem. Phys.* **68** 5325
[32] Kurtz S R and Stapleton H J 1980 *Phys. Rev.* B **22** 2195
[33] Askew T R, Muench P J and Stapleton H J 1984 *Solid State Commun.* **49** 667
[34] Augustyniak-Jablokow M A 2001 *J. Phys. Chem. Solids* at press